Department of Physics and Astronomy
University of Heidelberg

Bachelor Thesis
in Physics
submitted by
Laura Victoria Klein

born in Neuss (Germany)

2016

Measurements of Scintillator Fibre Tracker Mat Quality for the LHCb Tracker Upgrade

This Bachelor Thesis has been carried out by Laura Victoria Klein
at the
Physikalisches Institut in Heidelberg
under the supervision of
Prof. Dr. Ulrich Uwer

Zusammenfassung:

Während der Wartungsarbeiten 2019/2020 wird im LHCb Experiments am LHC in Cern der alte Spurendetektor durch den neuen Scintillating Fibre Tracker ersetzt. Dieser ist aufgebaut aus szintillierenden Fasern, die eine Dicke von 250 μm haben. Die Fasern werden zusammengefasst zu Fasermatten, die aus sechs Schichten der Fasern bestehen und eine Länge von 2,5 m haben. Jeweils acht Fasermatten werden zu einem Modul zusammengefasst. In der vorliegenden Arbeit werden diese Fasermatten und ein Prototyp-Modul untersucht. Der Detektor soll eine hohe Effizienz in der Teilchendetektion und Ortsauflösung haben. Um zu testen, ob mit den Fasermatten die Anforderungen erreicht werden können, kann die Lichtausbeute der Matten gemessen und untersucht werden.

Damit beschäftigt sich diese Arbeit. Dabei liegt der Fokus darauf, Schäden, die durch die Produktion entstanden sind und zu einer Qualitätsminderung der Matten führen, zu entdecken und bestenfalls die Herstellung zu verbessern, um weitere Schäden der gleichen Art zu vermeiden. Es wurde, aus denselben Gründen, auch der Prototyp eines Moduls untersucht. Die in dieser Arbeit angewendeten Methoden haben sich gut für diese Tests geeignet und sollen deshalb auch später in der Serienproduktion angewendet werden.

Abstract:

During the Long Shutdown in 2019/2020 the tracking system of the LHCb experiment at the LHC in Cern will be replaced by the new Scintillating Fibre Tracker (SciFi Tracker). The SciFi Tracker consists of scintillating fibres with a diameter of 250 μm. These fibres are built into fibre mats which consist of six layers of these fibres and are 2.5 m long. Eight mats are assembled into so called modules. In this thesis several fibre mats and a prototype module have been tested. For the new detector a high hit detection efficiency and single hit spatial tracking resolution are required. To test if the fibre mats fulfill these requirements the light yield is measured and analyzed.

This is described in this thesis. The focus lies on the detection of damages which appear during the production of the fibre mats and lead to a deterioration of their performance to improve the production. Also, a prototype module has been tested to look how good the module assembling is done. The methods which were used in this thesis showed to be able for this kind of tests and therefore will be also used later in series production.

Contents

1   Introduction

Over the last decades of the 20th century the Standard Model of particle physics (SM), which is an effective quantum field theory, has been developed. It describes the known elementary particles and fundamental interactions with great success, except gravity. Until now, it has withstood all experimental tests. Admittedly, there are some open questions left which the SM cannot explain, like neutrino oscillation and dark matter.

The environment to test the SM is provided by the Large Hadron Collider (LHC) which is located at CERN[1]. The four principle experiments installed there are ALICE, CMS, ATLAS and LHCb. Data has been taken since 2009. Currently, most measurements are limited by the statistics. Therefore, in 2019 LHCb plans to upgrade the detector to increase the data collection rate. An important part of the upgrade is the replacement of the downstream trackers by a new Scintillating Fibre Tracker because the old detector cannot handle the higher particle rate.

The new tracker consists of scintillating fibre mats constructed from several layers of scintillating fibres. Eight mats will be assembled into 5 m long and 0.5 m wide modules. Each of the 12 tracking layers will consist of 10 - 12 modules. This is described further in Chapter 3. For light detection, Silicon Photomultipliers will be used. Their pitch is adapted to the geometry of the fibres.

In this thesis work I will test some of the first fibre mats produced before the serial production started and examine if they perform as expected.

Defects in the fibre mats degrade the hit detection efficiency of the fibre mat and tracks.

Chapter 2 introduces the LHC project and especially the LHCb experiment while Chapter 3 describes the planned upgrade. The remaining chapters will describe the test methods and results. In Chapter 4, measurements of the light yield from fibre mats are described and analyzed for its homogeneity and amplitude across the mat to look for defects in production. In addition, the reflectivity of the mirror, which is glued on one end of every fibre mat has been tested. Special attention is paid to the edges of the mats. A final machining step for the fibre mats which removes excess fibres, can easily destroy the fibre mats at the edges and there is some potential to damage the mirror of the mat. This is described in Chapter 5. Chapter 6 presents the study of the performance of the fibres mats assembled into a module. The results are summarized in Chapter 7.

---

[1]Conseil Européen pour la Recherche Nucléaire

2 The LHCb Experiment at the Large Hadron Collider

2.1 Introduction

The **L**arge **H**adron **C**ollider (LHC) is a large proton and heavy ion collider located at CERN near Geneva, Switzerland [4]. It measures 27 kilometers in circumference. The ring accelerator reaches energies up to 13 TeV. It is running since 2009. There are four big main experiments, ATLAS, CMS, ALICE and LHCb. In Figure 2.1 an overview of the experiments is shown.
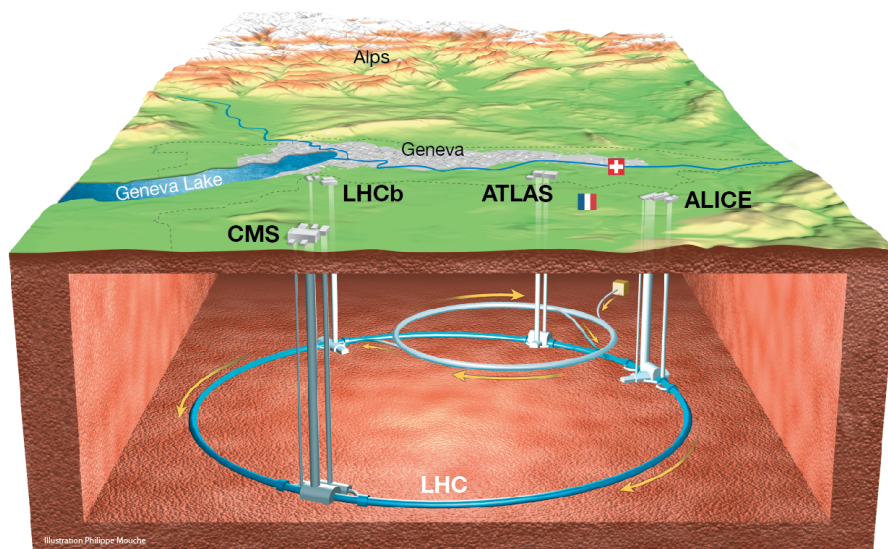

Figure 2.1: Overview of the experiments at the LHC in CERN [13]

ATLAS (**A T**oroidal **L**HC **A**pparatu**s**) and CMS (**C**ompact **M**uon **S**olenoid) are multi-purpose-experiments. They are designed to cover a broad research programs. They investigate, for example, possible substructures of the smallest known elementary particles, how the elementary particles got different masses and how the fundamental interactions can be combined to a quantum field theory that includes gravitation.
CMS also studies the collisions of heavy ions.
ALICE (**A L**arge **I**on **C**ollider **E**xperiment) studies heavy-ion collisions in which quark-gluon plasma is formed.
The LHCb (**L**arge **H**adron **C**ollider **b**eauty) experiment tests the Standard Model

of particle physics by searching for CP-symmetry violation which is one of the causes for the matter-antimatter-asymmetry observed in the universe.

Additionally, LHCb searches for rare decay processes with b- and c-mesons such as $B_s \rightarrow J/\Psi\ \varphi$. Decays like this provide a clean experimental signature and allow to test the standard model because of small theoretical uncertainty. Therefore, they are good candidates to discover deviations from the Standard Model prediction and provide evidence for new physics.

2.2   The LHCb Detector

The LHCb Detector is a single-arm forward spectrometer and covers 300 mrad of angular acceptance. This type of detector has been chosen because the b-hadrons are predominantly boosted in the forward and backward direction near the beam axis. The particles in the backward cone are not measured [3].

At the moment the detector consists of several subsystems:

- A magnet deflects the charged particles so that the momentum of the particle can be calculated when the trajectory before and after the magnet is determined.

- The so-called Vertex Locator (VELO) is a silicon-strip detector and located around the collision point. It measures the trajectories near the collision point.

- There are the two Ring Imaging Cherenkov Detectors (RICH). They are used to identifying particles by using the Cherenkov effect in combination with the tracking system. RICH1 is located before the magnet and RICH2 after it.

- The Tracker Turicensis (TT) and Tracker Stations (T1-T3) reconstruct the charged particle trajectories. The Tracker Turicensis is a silicon-strip detector placed before the magnet. The three Tracker Stations are located after the magnet. The Stations all consist of a silicon-strip based Inner Tracker (IT) surrounding the beam pipe and a gas straw-tube based Outer Tracker (OT) which covers the outer region up to 3m from the beam pipe in the horizontal direction.

- RICH2 is followed by the electromagnetic and hadronic calorimeters which reconstructes the energies of photons and electrons, and hadrons, respectively.

- The muon stations are the last substations which identify and measure the trajectories of the muons. Multi-wire proportional chambers are used for that purpose.

3 The Scintillating Fibre Tracker for the LHCb Upgrade

3.1 Motivation

Currently, LHCb results are limited by statistical uncertainties. The goal of the upgrade is to collect more data to reduce the uncertainties. It will be possible to collect an integrated luminosity of 5fb^{-1} data per year instead of $1\text{-}2\text{fb}^{-1}$ currently. A total of 50 fb^{-1} will be collected in 10 years [10].

At the moment, the maximum luminosity at which the LHCb experiment can be operated is limited by the bandwidth of the read-out system, the maximum occupancy the detector can handle and the risk of aging of the detectors. To allow the operation of the LHCb experiment at a luminosity of $\mathcal{L} = 2 \cdot 10^{33} cm^{-2} s^{-1}$ during the shut down in 2019 - 2020 several upgrades of the detector are planned. The front-end electronics will change to a 40 MHz read-out with a software trigger instead of a 1 MHz hardware trigger for event selection.

As well, some subsystems will be rebuilt or replaced. In Figure 3.1 the schematic view of the upgraded detector is shown.

The Tracker Turicensis will be replaced by the so-called Upstream Tracker and the Inner and Outer Tracker Stations will be replaced by the Scintillating Fibre Tracker (SciFi Tracker). The occupancy of the OT straw tubes would be too large such that the tracking efficiency begins to degrade, and therefore it must be replaced. Additionally, the IT was only designed to operate until 10 fb^{-1}. There are also several more projects for the upgrade which are not further discussed in this thesis.

3.2 The Scintillating Fibre Tracker

The SciFi Tracker is made from 0.250 mm scintillating fibres. Overall about 10000 km of fibres will be used. The SciFi tracker is constructed as 128 modules which consist of eight fibre mats each with a length of 2.424 m and a width of 13.045 cm. In total that means at least 1024 mats are necessary. Each fibre mat consists of six layers of fibres. The scintillating fibres are produced by the Kuraray company (Type SCSF-78MJ). The scintillating light is be detected with Silicon Photomultipliers (SiPMs) which are further described in Chapter 3.5. The SciFi tracker consists of three stations which each have four detection layers. In Figure 3.2, the front and the side view of a station are shown. Scintillating fibres, fibre mats and modules are described in detail in Chapter 3.3 and 3.4.

One detection layer is made of 10 - 12 modules. A module consists out of 8 fibre mats. The x-layers are vertical with respect to the y-axis. The u-layer is tilted by
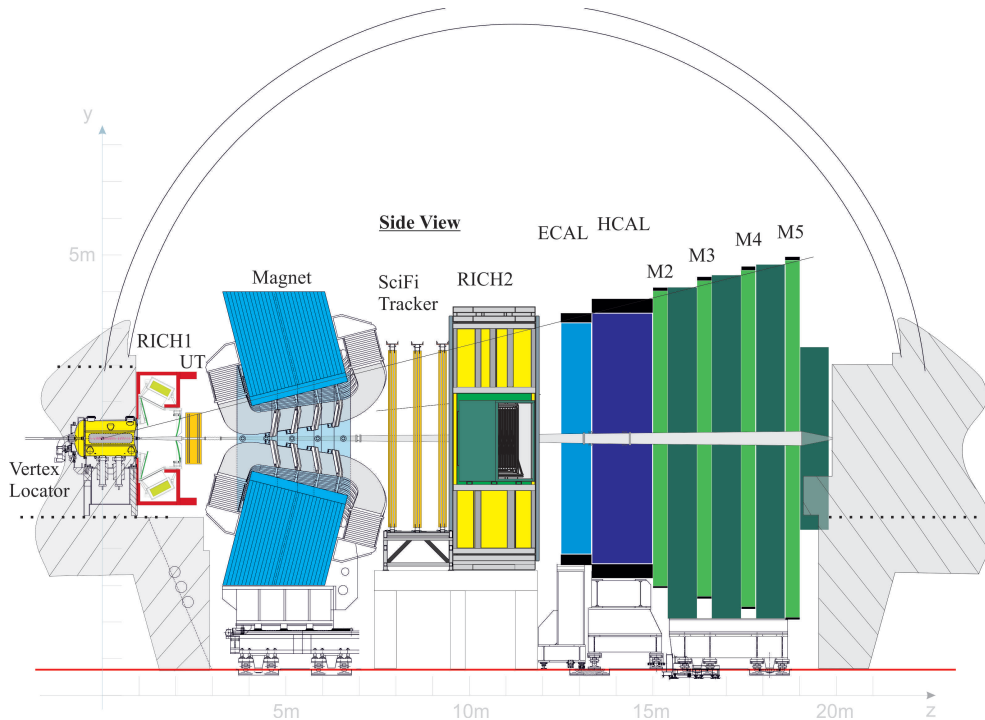
Figure 3.1: Schematic side view of the upgraded LHCb detector [1]

-5°, the v-layer by 5°. The center hole accomodates the beam-pipe.

The requirements for the SciFi Tracker are that the hit detection efficiency should be as large as possible, about 99%, while the noise cluster rate should be less than 10% of the signal cluster rate. The Clustering is explained in Cahpter 3.7. The single hit spatial resolution has to be better or equal to 100 μm in the x-direction. The electronics should run at 40 MHz and the recovery time of the read-out should be small to prevent too much dead time in data taking. The effect of multiple scattering should be as low as possible, therefore, the material in acceptance region should be minimized.

3.3   Scintillating Fibres

The active component of the SciFi tracker are the scintillating fibres. The fibres are plastic scintillators.

A scintillator exhibits scintillation when it is excited by ionizing radiation. They absorb part of the energy of the incoming particle and re-emits it in form of light. The time that passes until the light is re-emitted is called relaxation time. It can be delayed because the excited state can be stable for a certain time. The transitions happen through the free valance electrons of the molecules in organic scintillators.
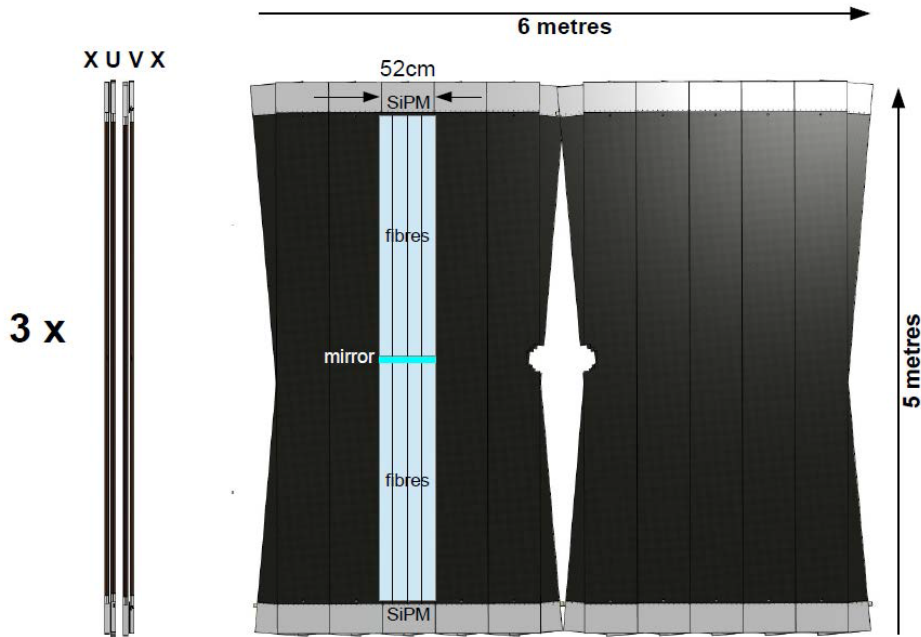
Figure 3.2: Schematic of the SciFi Tracker in yz- and xy-plane. One module is highlighted in blue and the segmentation of the eight fibre mats is indicated[8].

This process is similar to luminescence, but in this case the excitation is caused by ionizing radiation and not photons.

To excite a single molecule the deposited energy of the passing particles has to be some few eV. Typically $2 \frac{MeV}{cm}$ of energy is deposited in plastic by a minimum ionizing particle.

The wavelength spectrum and the decay time constant are important characteristics of a scintillator.

The base scintillating material of the Kuaray scintillating fibres used at the LHCb fibres is polystyrene which emits in the UV wavelength. Because the relaxation time would be too slow, a dopant is added to the fibre. P-terphenyl (PT) is used for the fibres used in the SciFi Tracker. Because UV light has a short range in most materials, a second fluorescent wavelength-shifting dopant has to be added. Here it is tetraphenyl-butadiene (TPB).

The energy transfer between the core and the dopants is due to the so-called Förster resonance energy transfer (FRET). The energy of an excited dye, called the donor, is transferred to a second dye, called acceptor. The transfer functions without radiation. That means there is no emission and absorption of photons but

a dipole-dipole-coupling. The donor induces an oscillation in the acceptor which can emit the transferred energy through radiation. The distance between the two dyes has to be very small, about a few nanometer, to make the mechanism work. Dopant concentrations are typically about 1%. This results in a fast and efficient energy transfer from the base polymer to the fluorescent dyes with a rapid emission ($\tau = 2.8$ ns) of a photon in the blue to green wavelength. The emission spectrum for this type extend from 400 to 600 nm. The peak is about 450 nm.
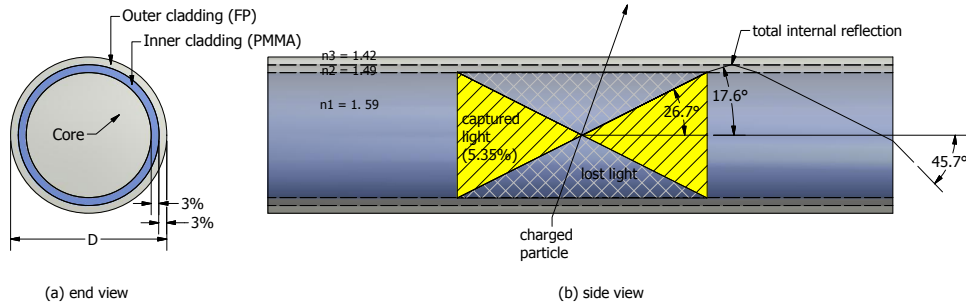

Figure 3.3: Schematic of the structure of a scintillating fibre from end view (a) and side view (b)

In Figure 3.3 the structure of a fibre can be seen. In consists of a polystyrene core, with an index of refraction of $n = 1.59$ Two claddings of lower indexes of refraction are used to trap light within the fibre core. The outer cladding consists of a fluoridated polymer cladding (FP), with $n = 1.49$. The inner cladding of the plastic polymethyl methacrylate (PMMA). Single clad fibres typically have an index of refraction of 3.5%.

Light Yield

As said before, the deposited energy of the passing particles has to be about $2 \frac{MeV}{cm}$. The scintillator used for this detector produces about 8000 photons per MeV. That means that about 300 photons are produced in a 250 μm fibre by minimum ionizing particles. A mat consists of six layers of fibres. Only 5.35% of the photons are captured through total internal reflection. Some of the photons are lost on their way to the SiPMs because of attenuation. The SiPMs have a photon detection efficiency of about 38.%. As a result about 15 photons are usally detected and converted into photoelectrons.

Attenuation Length

Attenuation describes the loss in intensity of a flux through a medium.
The attenuation length describes the distance λ for which the probability that a

photon has not been absorbed yet is $1/e$ or the intensity has dropped to $1/e^2$ which means that about 63% of the photons are already absorbed or scattered away. The intensity of the light after a distance x is then

$$I(x) = I_0 \exp\left(\tfrac{-x}{\lambda}\right) \tag{1}$$

The attenuation length for the fibres that are used for the detector is 300-350 cm when measured from 1 to 3 m. The attenuation length depends on the wavelength of the light as well as the purity of the polystyrene, and quality of the cladding surface.

3.4   Mats and Modules

3.4.1   Mat production

To produce an adequate light yield for nearly 100% hit detection efficiency, the scintillating fibres are wound into mats with six layers of fibres. They are cut to a final width of 130.45 mm and a total length of 2424 mm in order to cover the entire acceptance of the detector.

For the mat production, a winding machine similar to the one seen in Figure 3.4 [2, 8] is used.
There are currently four different production centers which produce the mats. The working principle is always the same. It is described in detail in [8].

The fibres are wound on a wheel which has a diameter of about 1 m. A milled thread on the wheel guides the fibres of the first layer. The next layers are placed in the grooves of the previous layers shifting by one half of the horizontal pitch.
The fibres are bonded with epoxy. By adding titanium dioxide as one component to the epoxy mixture, the optical crosstalk between the fibres can be reduced. The glue is hardened after one day.
In the center of the wheel surface are small holes every 25 cm which are filled with the epoxy mixture. This leads to small pins on the mat which are later used for alignment during module assembling.

To increase the light yield, a mirror is glued on one end after the ends have been cut to optical quality. The light will be read-out on the other end by the SiPM arrays.
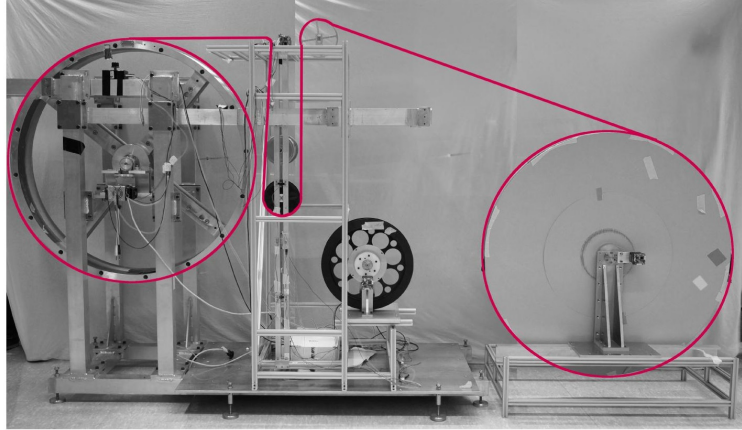
---

[2]e denotes Euler's number

Figure 3.4: Prototype of the winding machine. On the right is the fibre spool, the winding wheel is on the left. The tension is controlled by a smaller weighted wheel that can be seen in the middle. [2]
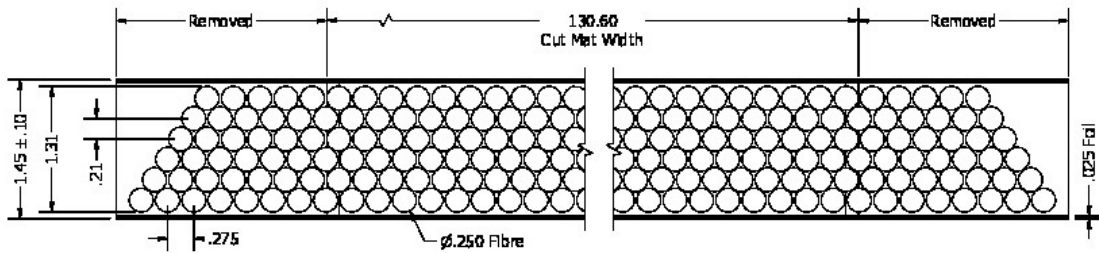

Figure 3.5: Schematic view of an uncut fibre mat with 6 layers. The sides will be removed so that the mat will have a width of 130.5 mm and a length of 2.5 m[2].

During the winding process some problems can occur. The fibres can jump during the winding so that they are missing fibres in the fibre matrix. It can also happen that there are cracks in the mats between fibres. This results in a shift in the location of the SiPMs versus the position of the mat. The position of the fibres can also be disturbed if the fibres have so called bumps, which means that there they are much thicker than 250 μm. These local defects in the fibre matrix result into degraded position resolutions.

In this thesis several mats have been tested to identify if these possible defects lead to a degradation in performance.

3.4.2   Modules

As shown in Figure 3.6, a module consists of 8 fibre mats with 4 mats end to end. Two half panels of honeycomb and carbon fibre skins are attached to each side for stiffness and protection. It is important that the module is in a light-tight frame so that no light can come in from the edges or surface causing noise hits in the detector. A black polymide foil covers all outer surfaces. Carbon-fibre reinforced sidewalls are added on the sides as well. The dimension of a detector module are 4.85 m x 0.528 m.

10 - 12 modules will then be grouped together to form a single layer of 8 - 10 normal modules and two special beam pipe modules. The whole SciFi tracker will contain 12 planes in three stations of X-U-V-X.

This leads to a number of more than 1024 fibre mats for the whole detector which must be tested and qualified.
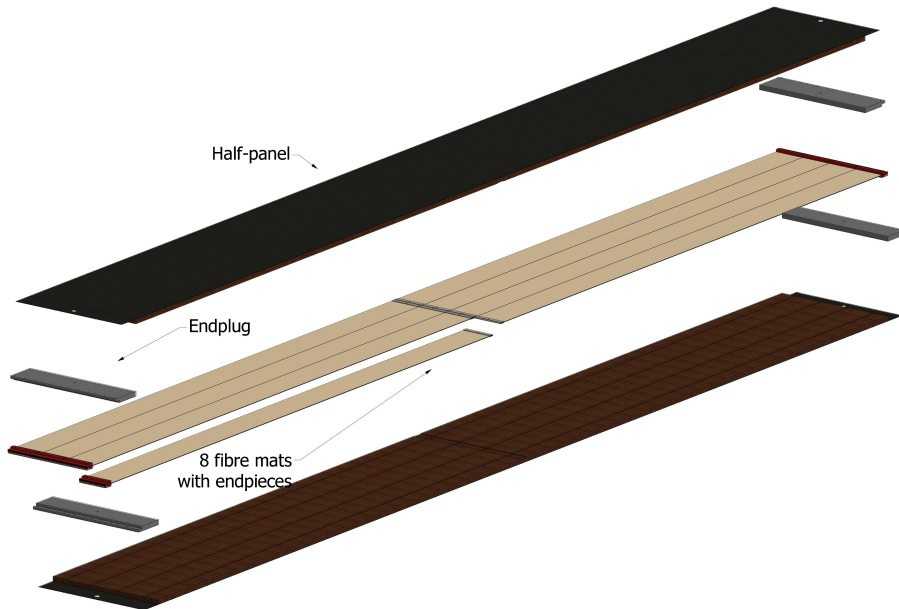

Figure 3.6: Exploded view of a module. The 8 fibre mats are placed with the mirror inside. The module is covered to guarantee light tightness [8].

Beam pipe modules have the same width, length and are operated in the same way but have the inner mat cut to shorter length to accommodate the beam pipe.

The fibre mats investigated in this thesis are produced at the RWTH Aachen and

the TU Dortmund.

The labeling is continuous and begins with FIM00001. The information about all fibre mats is collected in a database[3]. Longitudinal cuts and module production have been performed in Heidelberg.

3.5   Silicon Photomultipliers

The light produced by ionizing particles in the scintillating fibre mats is read out by Silicon Photomultipliers (SiPM). They are installed at the end of the mat opposite to the mirror. The SiPMs used for the studies described in this thesis and later in the tracker are produced by the Japanese company Hamamatsu. Their operating mode is discussed in section 3.5.1 and 3.5.2. One SiPM has 128 channels. It consists of two 64 channel silicon dies. In between is a small gap that has the size of one channel. One channel contains 4x24 pixel. There are different versions of the Hamamatsu SiPMs. The ones used for this thesis are called for simplicity the 2014 and the 2015 chips. The dimensions of 62.5 μm x 57.5 μm. One channel has the size of 250 μm x 1620 μm each, in the 2015 version, used for the module measurements. For the measurements in Chapter 4 and 5 the 2014 versions are used with 250 μm x 1520 μm.
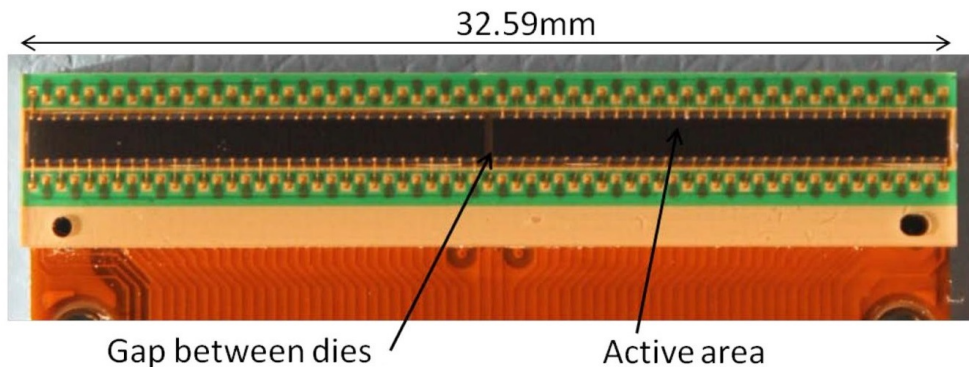

Figure 3.7: Overview of one SiPM array. The gap between the two dies can be seen [1].

3.5.1   Avalanche Photodiodes

Each pixel of the SiPMs consists of an avalanche photodiode. A photodiode converts the detected light into a current which is measureable by the electronics. It

---

[3]`https://scifi.physi.uni-heidelberg.de`

is based on the principle of semiconductors. An extrinsic semiconductor is used with p-n junction. The free electrons from the n-part diffuse to the p-part which leads to a current. The holes diffuse in the opposite direction. An electric field is built up which stops the diffusion. Now the p-type and n-type sides are occupied with a negative and positive charge densities.

This is already a simple form of a diode. When an external voltage (U_{Bias}) is applied, in one direction the resistance is negligible (forward bias operation), whereas in the other direction a current can only flow if it overcomes the internal filed (reversed bias operation). The voltage it has to overcome is called breakdown voltage (U_{BDV}).

3.5.2 Working Principle of the SiPMs

Because the pixels of the SiPMs used for the set-ups in this thesis are very small it is very unlikely that two photons hit the same pixel. The number of pixel is large compared to the number of the photons. That means that the SiPMs can count single photons, so the number of firing pixel is proportional to the number of arriving photons.

The incoming photons create electron-hole-pairs in the intrinsic semi-conductor by depositing their energy in the drift region. The drift region lies between two doped areas. A reversed bias voltage is applied to make the electrons drift to the multiplication area (p-n$^+$). There are more electron-hole-pairs produced.

There are two modes diodes can be operated - the linear and the Geiger mode. In the linear mode the bias voltage is below the breakdown voltage so the current is proportional to the light intensity. In the Geiger mode the bias is voltage is above the breakdown voltage. In this mode an electron-hole pair produces an avalanche of more electron-hole-pairs.

The SiPMs are operated in this Geiger mode. A quenching resistor in the SiPM reduces the voltage once a current flows, stopping the avalanche.

In Figure 3.8 it can be seen that the height of the incoming pulse is depended on the number of photo electrons which are induced by the incoming photons. It is clearly distinguishable how many photo electrons arrived. That means the signal amplitude can be measured.

3.5.3 Characterization

The different parameter of SiPMs are described in the following:

Breakdown Voltage

The breakdown voltage describes the voltage that is needed to create avalanche. The SiPMs are operated at the over-voltage. It is defined as

$$U_{OV} = U_{Bias} - U_{BDV} \tag{2}$$

The breakdown voltage is depends on temperature with the coefficient $\kappa = 53.7$ mVK^{-1} with
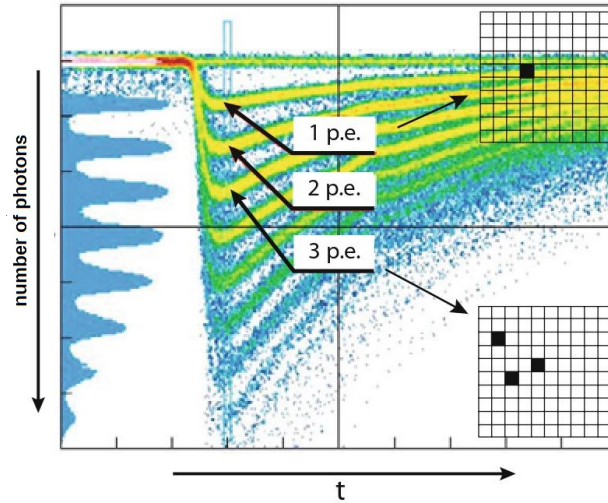
$$U_{BDV} \propto \kappa \cdot T \tag{3}$$

Figure 3.8: Pulses for different numbers of firing pixels. [12]

Gain
The Gain is the multiplication factor of the elementary charge inside the avalanche.

$$G = \frac{Q_{avalanche}}{e} \tag{4}$$

The charge of the avalanche is described by $Q_{avalanche} = U_{OV} \cdot C$. C is the capacitance of a pixel. The higher the gain the better can the signal be separated from electrical noise.

Dark-Count Rate
Because of the thermally generated noise - thermally excited electrons can trigger avalanches - of the SiPMs there is a dark count rate. They are of the same amplitude as a single photon generated avalanche. The rate is dependent on the over-voltage and can be made worse by radiation damage.

Crosstalk

Crosstalk is the pixel to pixel crosstalk which is produced by infra-red photons created during the avalanche. Single photoelectron signals appear as two or more. The probability is dependent on the over-voltage.

Photon detection efficiency (PDE)

The PDE is defined as the ratio between the detected photons and all incident ones.

It is dependent on the geometrically active area of the pixel and the probability that the incident photons create electron/hole-pairs. The probability of the primary photon to trigger the avalanche is dependent on the over-voltage and the wavelength (see Figure 3.9).
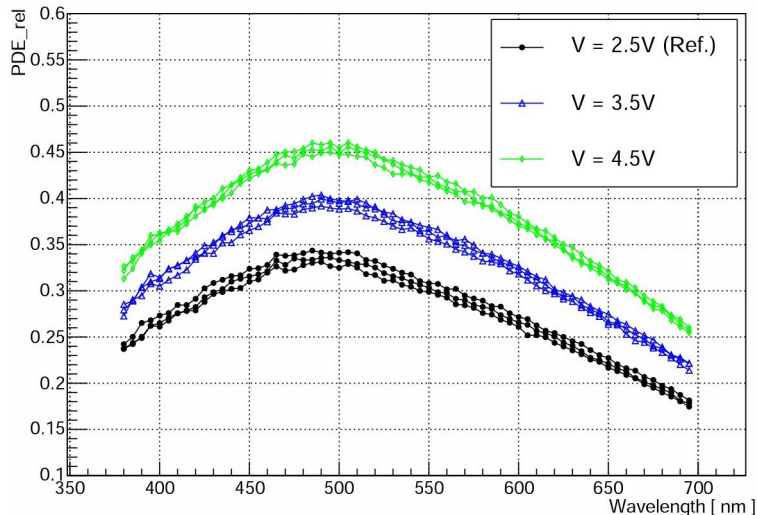
Figure 3.9: PDE for different over-voltages. The peak for $U_{OV} = 3.5$ V is at the wavelength of 490nm with 39% [2]

3.6 PACIFIC

The PACIFIC (Low **P**ower **A**SIC for the **SCI**ntillator **FI**bres Tra**C**ker) chip is developed to amplify, shape and digitize the analog signal from the SiPM [11]. It is designed to sample a rate of 40 Mhz. One PACIFIC chip will read out 64 channels, which is one half of a SiPM array[4].

In Figure 3.10 the schematic of the PACIFIC is shown. The signal from the SiPM goes through a preamplifer and is then shaped. Two interleaved gated integrators

---

[4] It is not used in the measurements described in this thesis since the PACIFIC is currently in development. Instead, the SPIROC chip will be used which is described in Chapter 4.2.1

are components of the PACIFIC. They integrate the charge signal. Then the signal gets digitized. The PACIFIC contains three comparitors for each channel meaning. Three thresholds can be compared to each charge signal (low, medium, high). Four results are possible (00,01,10,11). Therefore, it will be represented as 2-bit code.
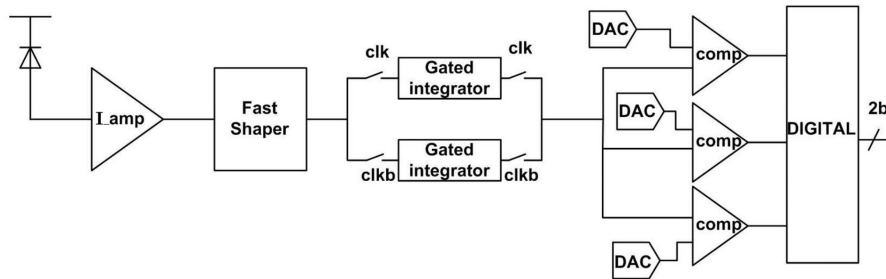

Figure 3.10: Schematic of the stages of the readout of one channel [1]

3.7   The Cluster Algorithm

In the SciFi tracker the charge information from each channel will not be collected. As there are more than 500000 channels, read-out data reduction is necessary in order to reach a read out of 40 MHz. This is done by applying a so called cluster algorithm.

In general a charged particle creates a signal not only in one channel of the SiPMs but also in the neighboring ones depending on the angle the particle hits the fibre mat. In Figure 3.11 the shown particle crosses only one channel but due to crosstalk also pixels of the neighboring channels fire.

In the PACIFIC asic there will be three thresholds defined, a low, a middle and a high threshold to separate the data from noise. At least one channel has to pass the middle threshold. This is the so called seed threshold. If the neighboring channels pass the low threshold, they are also counted.

These signals are summed up and calculated in the mean channel. Less than 10 % of the clusters contain only one channel.

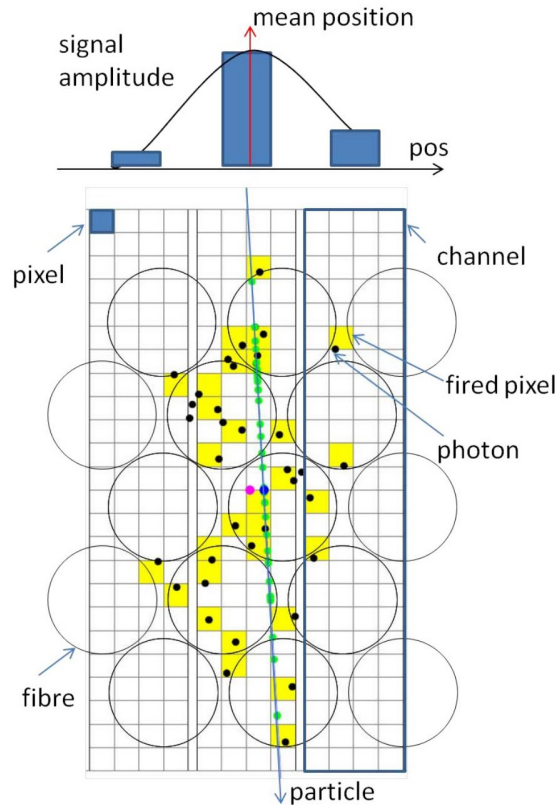This means that the information for each channel can be described by one of four possibilities.

Figure 3.11: Schematic of a particle passing a fibre mat with five layers. The signal amplitude is proportional to the total number of firing pixel as one pixel can detect one produced photon. The fibres are not aligned to the channels.[1]
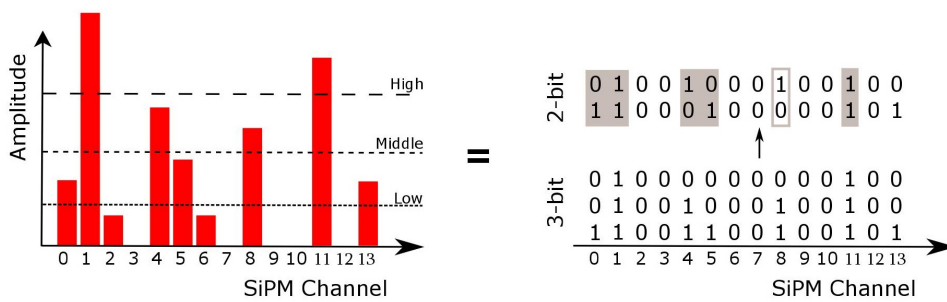

Figure 3.12: Left: Channel Clustering with three thresholds, right: 2-bit and 3-bit representation of it [2]

If the signal is lower than the low threshold, this channel will have the signal 00.

If it passes the low threshold but not the middle the signal is 01, for passing the middle but not the high it is 10. When passing the high threshold, it is 11.
Then the barycenter of the cluster will be calculated. The summation of the light yield of the whole cluster will then be calculated at the barycentred channel.
The algorithm has a maximum size of clusters which is four channels. Clusters wider than that have a possibility of 2.6%.

The PACIFIC chip is currently in development. For the measurements in Chapter 4 another asic is used which has the advantage that it can read out the signal amplitude. A similar cluster algorithm is applied in the read-out software[5].

---

[5] The software has been developed by Roman Greim and can be found by using the following link: `https://gitlab.cern.ch/lhcb-scifi/scifiusbboard/tree/master/utils/strosmic90`

4 Fibre Mat Light Yield Measurements

It is very important that the SciFi Tracker fulfills the requested requirements. That means that the hit detection efficiency and the spatial resolution have to be as high as possible. This variables cannot be measured easily in a labor but former measurements indicated that a high and homogeneous light yield is a sign of that. So to have a first look to the signal the fibre mats produce, the light yield produced by a beta-source is examined. The light yield measured is the mean amplitude of the signal measured in units of photoelectrons.

In the first setup, the light yield of the fibre mats is measured. It is important to test if this setup really is capable of testing the fibre mats, and finding the defects that will degrade performance. Then all fibre mats can be measured in order to ensure that later in the SciFi tracker the tracking resolution and efficiency is as high as required.

4.1 Experimental Setup

The test setup consists of a jig in which the mat is mounted with pins showing up. Back at the mirror end the trigger system and the source are placed. At the front the SiPMs are aligned so that they touch the readable side of the mat. No optical grease is used, only an air gap exists. The SiPMs are then connected to the front-end electronics. A 3 MBq Strontium-90 beta source is used.

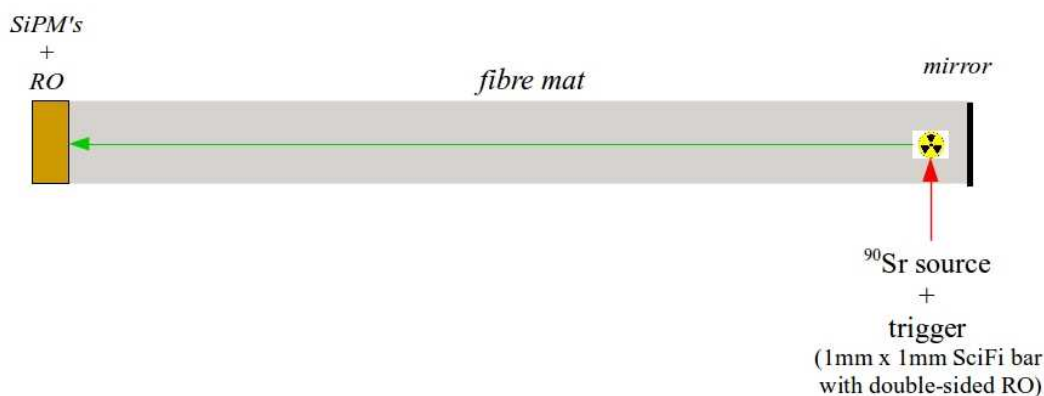In Figure 4.1 a sketch and in Figure 4.2 a photo of the set-up is shown.

Figure 4.1: Sketch of the experimental setup

Figure 4.2: Photo of the experimental setup

4.2 Front-End Electronics

4.2.1 SPIROC-A

The **S**ilicon **P**M **I**ntegrated **R**ead **O**ut **C**hip-Analogue or also called SPIROC-A is the read out chip which is currently used to read out the SiPMs [2]. Later in the SciFi Tracker the PACIFIC chip will be used instead. The advantage of the SPIROC chip is that the signal amplitude can be read.

One chip consists of 32 channels. The chip has four main components - a variable gain preamplifier, a programmable shaper, a track-and-hold-stage and an output. Eight SPIROC-A chips are mounted on a front-end card, such that two SiPMs can be connected to each front-end card. The SPIROC-A chip enables to tune the SiPM operation voltage for each single channel. This is very important because the different intrinsic breakdown voltages lead to different photon detection efficiency per channel if the operational voltage is the same for all channels. The range for this tuning is 4.5 V.

4.2.2 USB Board

The USB Board is for the read-out and powering of the front-end electronics [2]. The SPIROC and the USB Board are a **d**ata **a**cquisition **s**ystem (DAQ). It can read out different types of ASICs (**a**pplication-**s**pecific **i**ntegrated **c**ircuit) which

are similar in structure like the SPIROC-A.

The structure of the USB Board is visualized in Figure 4.3. The SiPMs are connected to the USB-Board over the uplinks.
One USB-Board can read out 8 uplinks simultaneously. Two uplinks are needed to read out one fibre mat. That means with one USB Board it is possibly to read out 16 SiPMs or half of a module.
The signal from the uplinks gets digitized by the 12-bit ADCs. The signal goes to the FPGA (Field Programmable Gate Array). In the uplink integrated there are also the power supply signal for the read out, the biasing voltage for the SiPMs, the DAQ trigger signal and the SPI signal.
The High Voltage supplies can give two operational bias voltages for the SiPMs.
The USB Board can work with an internal trigger or an external trigger. The Self-Trigger-Mode is used for taking the pedestal and the light calibration. It is created by the FPGA (Field Programmable Gate Array).
For taking the data of the particles it is necessary to use an external trigger. When the signal from this trigger arrives at the USB Board the USB Board sends a Busy signal to the trigger.
The USB Board can be connected to a PC and so the final data can be read out. The event rate taken by a USB Board is limited to 1.5 kHz.
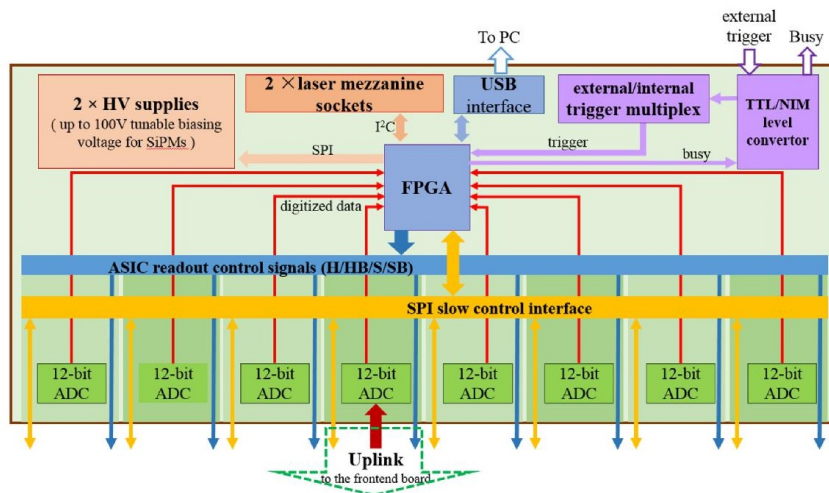
Figure 4.3: Buildup of the USB-Board [2]

31

4.3   Trigger System

The trigger used in this setup is a scintillating bar of the dimension 1cm x 1cm x 15 cm. On each side there are read-out electronics. A single channel SiPM detects the optical signal on either end. The electronics amplify the SiPM signal, discriminate the signal from each and also form a coincidence. The TTL signal from the coincidence trigger is converted to a NIM signal the USB Board can read later. After that, the signal passes the delay unit. Before the signal goes into the USB Board, it has to pass a logic unit. The signal only goes further to the USB Board if the Board is not busy.

The trigger scintillator is covered by 1 mm of plastic to absorb low energy betas that have passed through the fibre mat, ensuring only electrons with an energy about 1 MeV are triggered on.
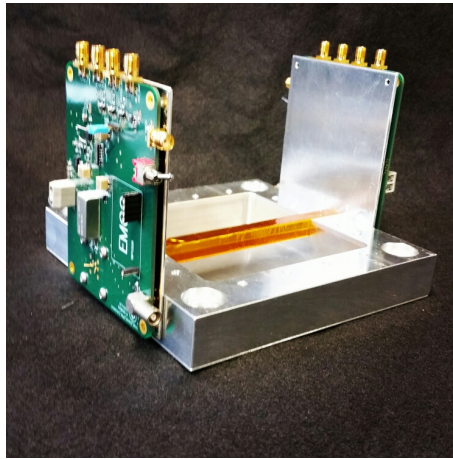
Figure 4.4: Trigger used for the setup to measure the light yield of the fibre mat. The bar which is covered in kapton tape is the scintillator. The green PCBs hold the read-out electronics

4.4   SiPM Calibration

In order to guarantee a homogeneous PDE (photon detection effiency) across the 512 channels of the four Silicon Photomultiplier arrays have to be calibrated.

Each channel of a SiPM has a slightly different intrinsic breakdown voltage. This results in different over-voltages for individual channels in case all channels are operated at the same voltage. The difference can be up to 0.5 V. This is a problem because a different operational voltage causes a different PDE and, hence, a different measured light yield.

To prevent this, the breakdown voltage of the SiPMs can be tuned in every single

channel by the SPIROC. However, an optical signal must be injected to all 512 channels such that a comparison can be made for the calibration.

Light bar Test

So-called light bars have been developed in Heidelberg for this calibration. The light injection bars are produced by handwork by scratching a fibre sideways to obtain homogeneous light. This light is then injected in the polycarbonate parts glued to the fibre mat. A picture of such a light bar can be seen in Figure 4.5.

Figure 4.5: Picture of a light bar

To ensure that the used light injection bars produce a uniform light yield for the measurements, they were tested the described setup. The internal trigger of the USB Board is used for that measurement.

In Figure 4.6 the ADC spectrum of the light of one channel of a SiPM can be seen. The first peak belongs to the pedestal. The second is the first photopeak. The system is adjusted, such that the first real photopeak is approximately as high in amplitude as the pedestal and up to 5 photopeaks can be seen. From this data, the SiPM gain can be determined.

When looking to Figure 4.7 the spectrum of the light can be seen in a 2D diagram for all 512 channels. The channels are displayed in the x-axis, the light signal in ADC values on the y-axis and the incidences on the z-axis. The light should be more or less homogeneous over all channels.

In Figure 4.7, it is shown how a good functioning light injection bar looks in the data. Four to five photo electron bands can be seen across all 512 channels. The
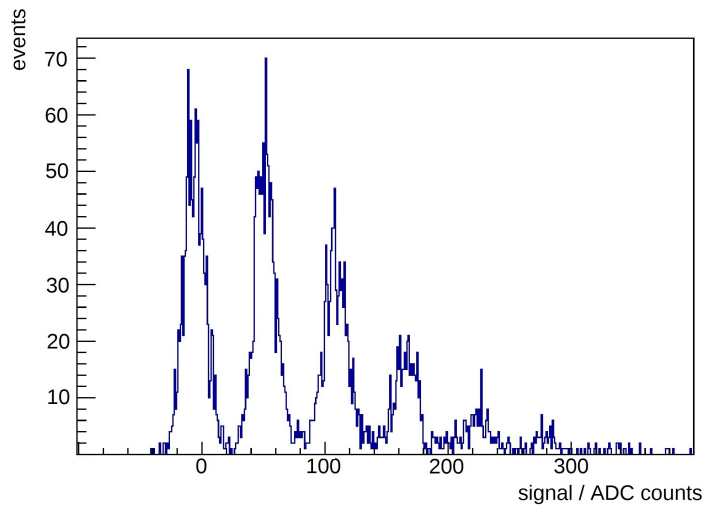
Figure 4.6: Spectrum of the light for one channel of the SiPM

data for Figure 4.7 and 4.8 was taken after the gain calibration of the SiPMs.

In Figure 4.8 a bad example can be seen. The produced spectrum is not homogeneous and only two photopeaks can be seen. In total over 40 light bars have been tested.

Gain Measurement

Firs,t the gain has to be measured for different bias voltages and for each channel. Therefore, the ADC spectrum has to be taken. The peaks come from the photoelectrons. A Gaussian is fitted on the peaks. The distance between the peaks is proportional to gain.

Determination of the Breakdown Voltage

The different voltages are plotted against the measured gain. By fitting a linear function to the data the breakdown voltage can be found out by extrapolating the linear function, as seen in Figure 4.9. The intersection point with the y-axis gives the result.
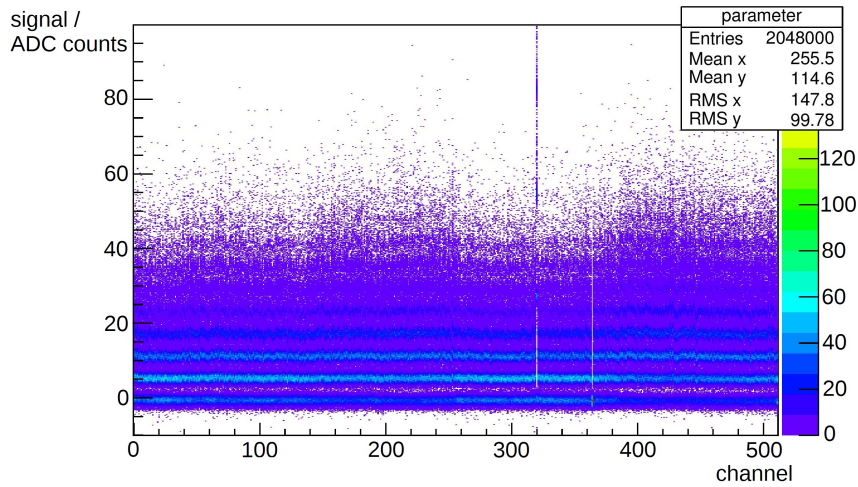
Figure 4.7: Spectrum of the light for all channels for a good light bar
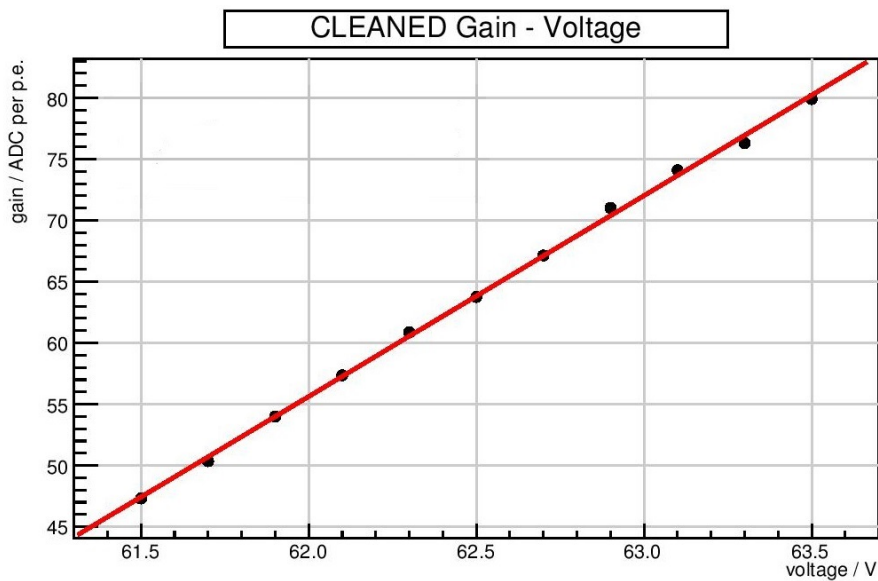
Figure 4.9: The Gain per ADC value is plotted against the operational voltage. With a fit the line can be extrapolated. The intersection point with the y-axis gives the breakdown voltage.

This is done separately for every channel. The result for every channel before the gain calibration is plotted in Figure 4.10.
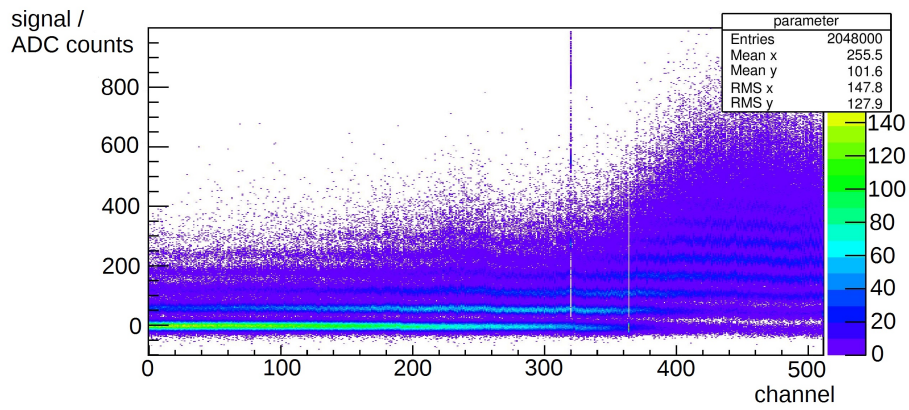
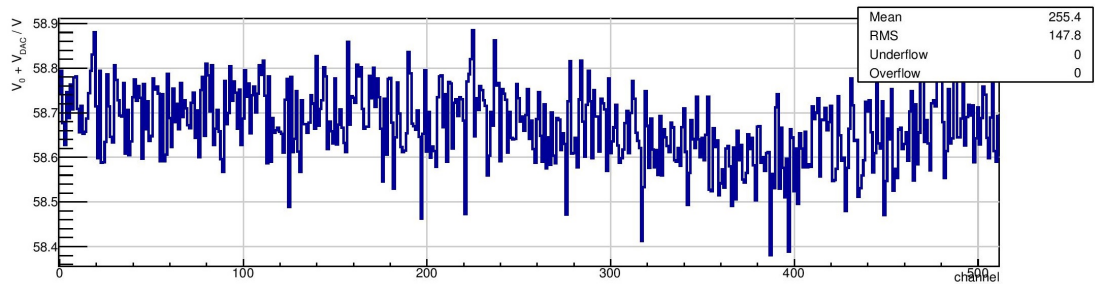Figure 4.8: Spectrum of the light for all channels for a bad light bar

Figure 4.10: Measured breakdown voltages for every channel before gain calibration
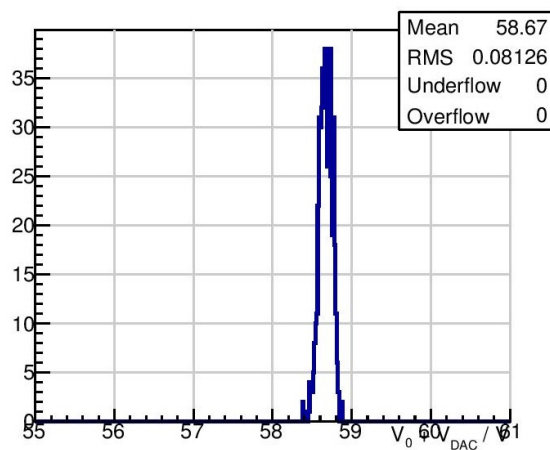
Figure 4.11: RMS for the breakdown voltage over all channels before gain calibration

The RMS of the plot in Figure 4.10 is shown in Figure 4.11.

The intrinsic breakdown voltages for every channel and the RMS after the gain calibration are shown in Figures 4.12 and 4.13. The range of the intrinsic breakdown voltages got smaller.
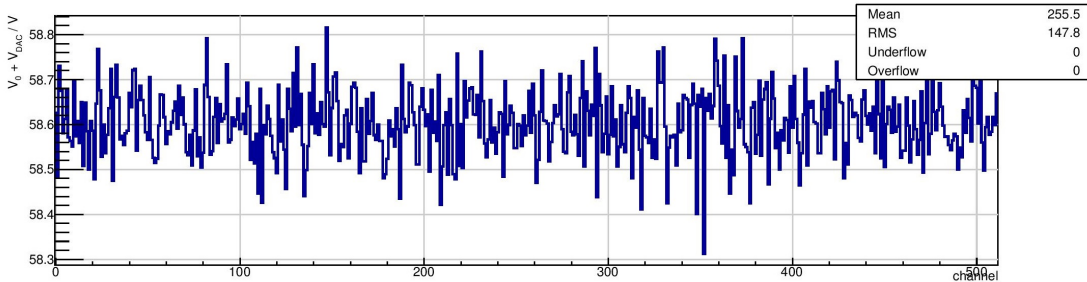
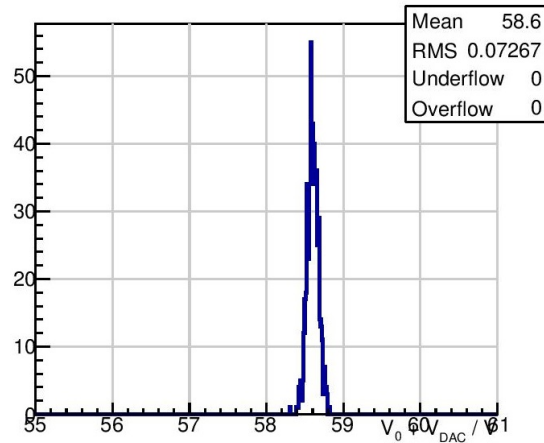Figure 4.12: Measured breakdown voltages for every channel after gain calibration

Figure 4.13: RMS for the breakdown voltage over all channels after gain calibration

By knowing the breakdown voltage of each channel the DAC values of the SPIROC can be tuned.

4.5   Light Yield Results

For all received fibre mats the light yield across all channels has been measured. In the following it will be discussed how the light yield should look like and what are the reasons for deviations.

In Figure 4.14 there can be seen an example with the fibre mats FIM00027 and
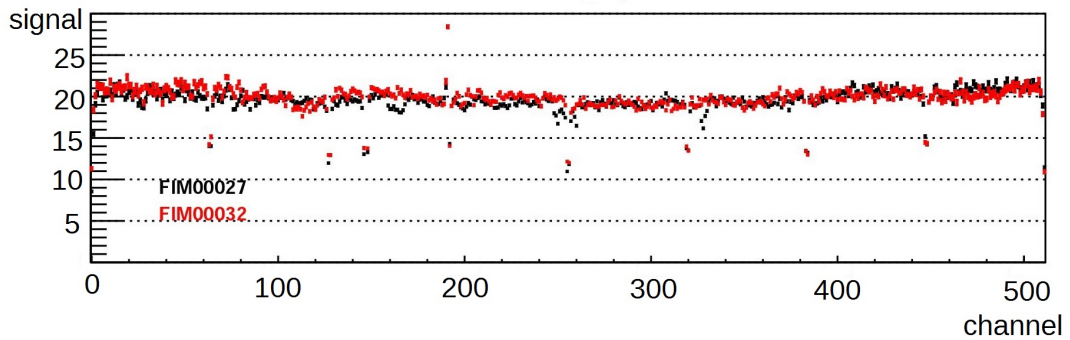FIM00032.

Figure 4.14: Measured light yield of the fibre mats FIM00027 and FIM00032.
Their average is used as reference mat.

These mats are used as reference mats. There are some noticeable structures in
the light yield data.
Every 64th channel has a lower signal. This is due to the gaps between the chips
of the SiPMs. Some signal passes through the area of these gaps and cannot be
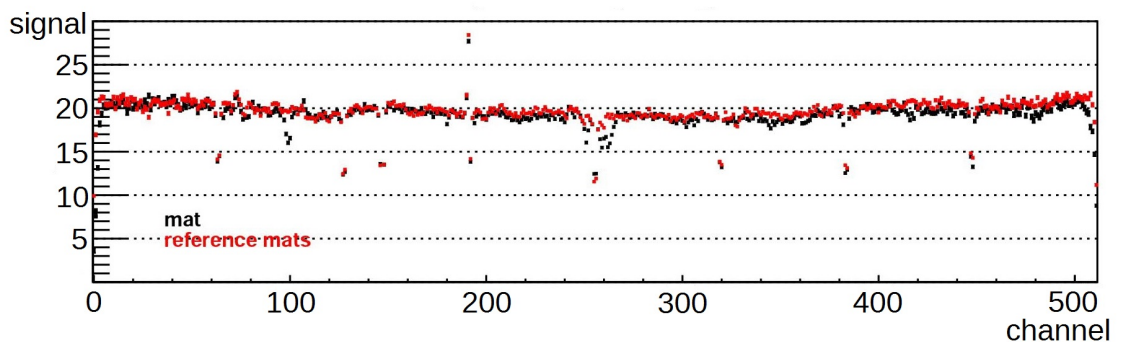detected.

Figure 4.15: Light yield of mat FIM00025 in comparison to the reference mats
FIM00027 and FIM00032

At the edges the light yield is lower. Part of this effect is due to the cluster algo-
rithm, this effect will be discussed later in Chapter 5. One other reason is that the

photons at the edges only pass partly through the fibre mat. That means not the whole signal can be detected. Another reason can be that the longitudinal cut was not done very precisely. The following chapter will go deeper in this cut analysis. The artifact near channel 200 is due to the SiPM which has a defective channel.

In the light yield graph in Figure 4.15 there is an artifact in the middle of the mat between channel 245 and 255. This was suspected to be due to the glue-type of the pins. This problem was solved after this discovery by using another glue. This was the first indication that this measurement is sensitive to detect defects in the fibre mats and effective to give feedback to improve the process of producing fibre mats.
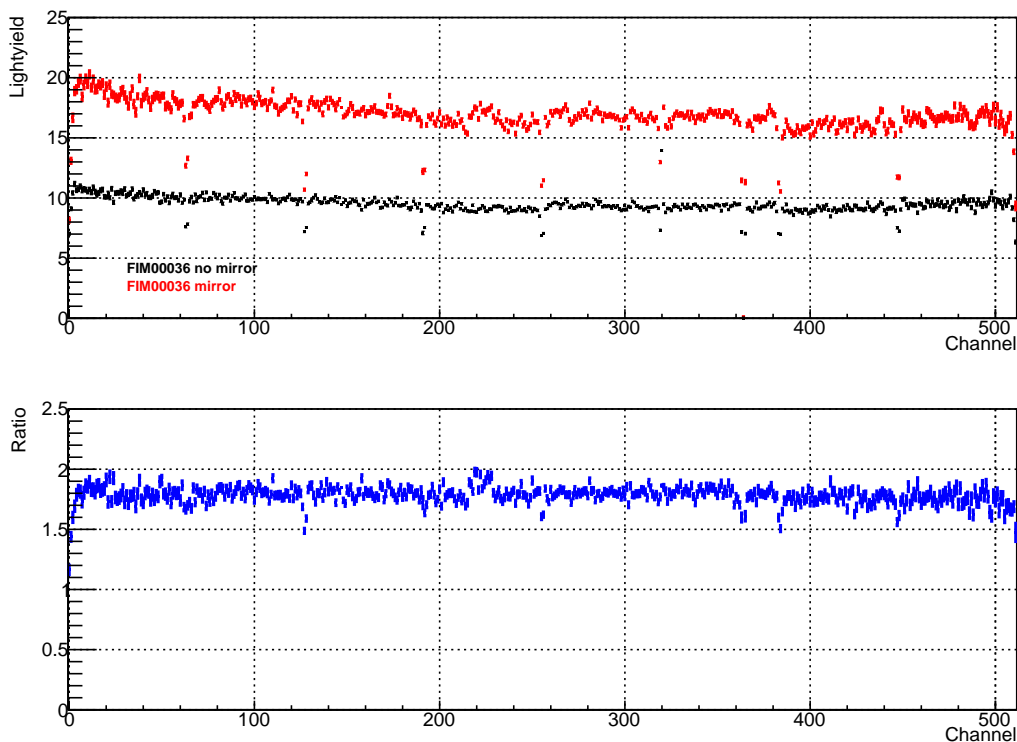
4.6   Reflectivity of the Mirror and Defects

Figure 4.16: Top: Light yield of mat FIM00036 with (red) and without (black) mirror
Bottom: The ratio between FIMooo36 with and without mirror

39

To get an adequate light yield, it is necessary to decrease the loss of photons. Therefore a mirror can be used. Early mirror foils consist of mylar foil (60 μm thickness). They are vacuum coated at CERN with an Al/MgF2 pair (90 nm/20 nm thickness) coating. Epotek H301-2 epoxy glue is used to bond the mirrors. This is the same epoxy used during winding [2]. The expected gain from the mirror is about 70%.

Later mats use an ESR (Enhanced Specular Reflector) film from the company 3M. The reflectivity is quoted as 98%, but the gain seen is typically about 80%. [14]

The light yield has been measured before the mirror has been attached and afterwards and the ratio has been calculated.

In Figure 4.16, there is an example for a ESR mirror. About 80% more signal has been gained which is what has been expected.

The first produced fibre mats have not been tested before the mirror has been attached. During the process of production the mirror can get damaged. In Figure 4.17 it can seen that the structure of mat FIM00028 looks very different from the others.
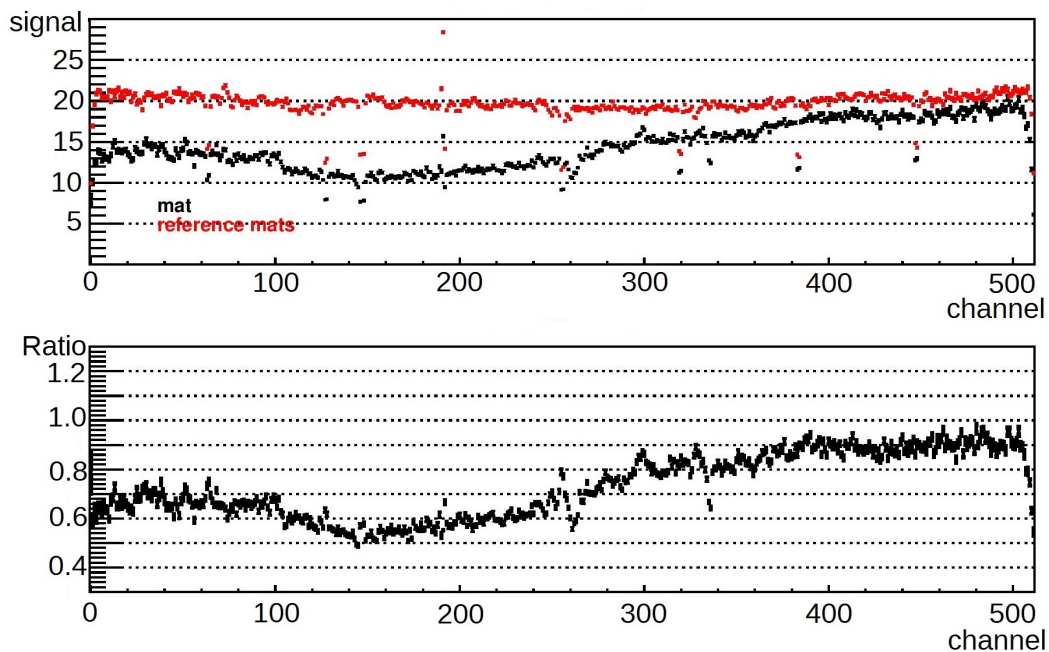

Figure 4.17: Top: Light yield of mat FIM00028 (black) in comparison to the reference mat average of FIM00027 and FIM00032 (red)
Bottom: The ratio between mat FIM00028 and the reference mat average

This effect could also be explained by a misalignment of the SiPMs for the measure-

ment of FIM00028. The misalignment leads to a lower light yield in the affected area because the SiPMs do not get the full signal. For this mat this was not the case because the structure was there even after realignment.

So the strange structure could be due to a mirror damage. That can not be investigates in measurements because they was no data taken before the mirror attachment.

In Figure 4.18 the mirror can be seen. Obviously a part of it has lifted. It is marked with the red box. During module production, the mirror will not be visible visually.

By comparing the damage that can be seen with the eye and the data in Figure 4.17 it is likely that the position from about channel 100 to 250 fits and therefore the damage has to be the cause for the loss of light yield in the data.
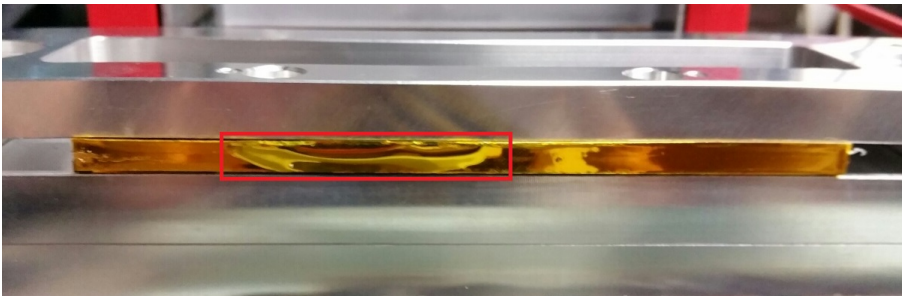

Figure 4.18: Mirror damage after the longitudinal cut of mat FIM00028

That shows that this method is sensitive in detecting such damages, so it is very important to test the fibre mats before attaching the mirror.

5 The Longitudinal Cut - Quality Assurance

The fibre mats are produced overwidth and must be cut to the correct width. The longitudinal cut has to be done very precisely to ensure that later the mats fit exactly in the module and no outer fibres in the mat are damaged. The appropriate width has to be reached within a tolerance of 150 μm over the mat's length of 2.42 m. The glue pins on the mat are used to align the mat during cutting and module production. In Figure 5.1 a schematic of a fibre mat can be seen. The alignement pins are good visible. In the alignment jig for the longitudinal cut 5.2, misalignment of the mat during cutting could produce cut fibres inside the final produced mat.
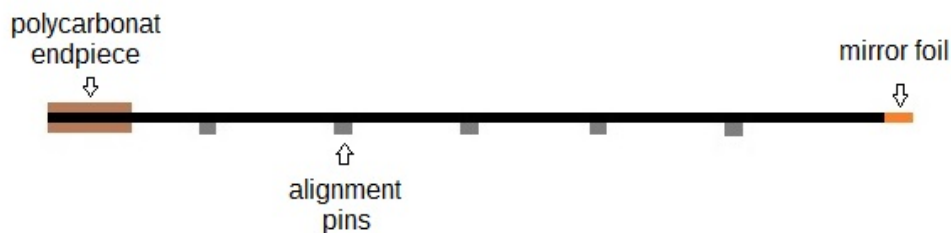

Figure 5.1: Schematic of a mat. The pins are used for alignment.

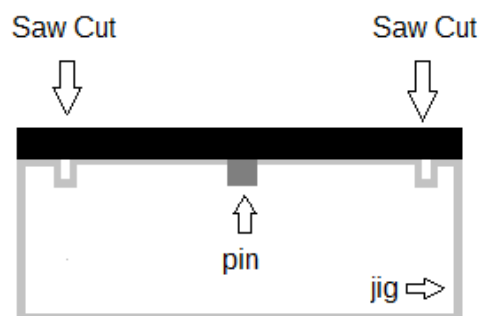The cut is done carefully with a professional milling machine.

Figure 5.2: Schematic of the longitudinal cut set up. The pins are used for alignment. A saw cuts away the excess fibres.

For the tested mats the longitudinal cut was done here in Heidelberg. The mirror

was already glued before the cut and additionally fixed with kapton tape.

In the Quality Assurance Measurements the edges of the fibre mats have been examined to see if there were fibres cut during the process and the mirror to see if the mirror was damaged. This is described in the subsequent sections.

5.1 Optical Inspection

A first indication that the fibres or the mirror at the edge of the mat have been damaged is seen in the optical inspection. A picture of the fibre mat edges is taken with a high resolution camera (Dino-Lite Premier AM7013MZT).

In Figure 5.3 you see an example for the optical photo. It was taken from mat FIM00043.

(a) Taken from the left side with the pins up. A very good example for a mat that is rarely affected by the cut.
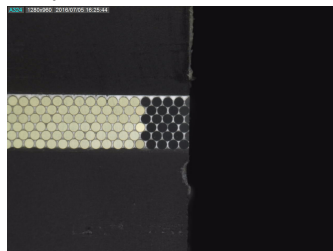
(b) Taken from the right side with the pins up. The fibres or the mirror at this edge is clearly damaged.

Figure 5.3: Optical photo of mat FIM00043

The light colored fibres show the reflected light from the camera. As one can see the left side looks good but the right side seems to be extremely affected by the cut. This is bad because in this region the light yield will be lower or even zero, depending on what is damaged - the fibres or the mirror. This leads to a lower particle detection efficiency. Probably about five to six channels will be affected

in the data for the right side.

This first impression has to be quantified with additional measurements.

5.1.1 Light Yield Ratio

To further investigate the defects at the edges the light yield measured with the QA setup from Chapter 4 before and after the cut has been compared by taking the ratio between these two measurements.

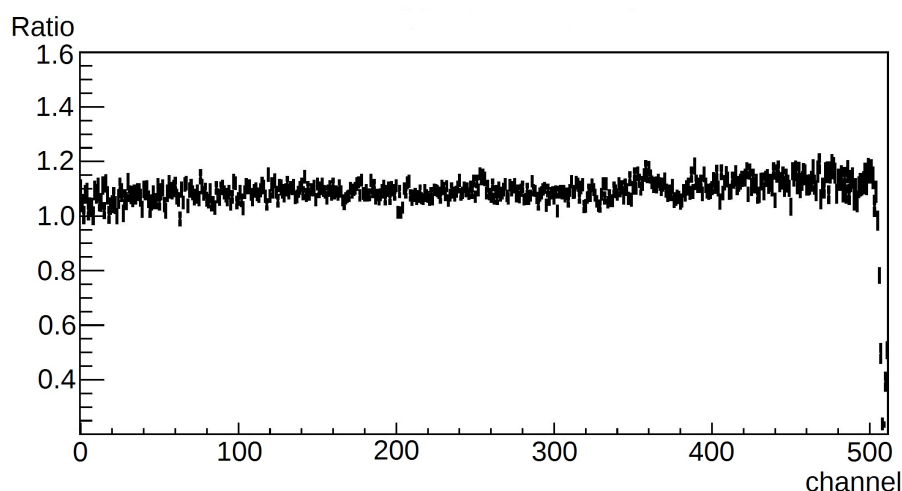In Figure 5.4, the ratio for mat FIM00043 is shown.

Figure 5.4: Ratio between the light yield of cut and uncut mat FIM00043

It seems like there is clearly damage at the right edge. About six channels at the right side seem to be affected. It could be that the mirror has been damaged and does not reflect the light at the edge anymore. In that case a ratio about 0.6 would be expected. If the fibres have been broken, the ratio should be around zero. The values seen in Figure 5.4 are in between zero and 0.6 but additionally there is another effect at the edges which must be considered. Due to the cluster algorithm the light yield at the edges is lower as there is some missing part of the cluster. That is because when the light passes the end and would create theoretically a signal in the neighboring channels but because the mat ans SiPMs end, the signal is not detected.

That is why the ratio from the light yield on a channel basis should also be calculated without the cluster algorithm. This will be done in the next section.

5.2   Ratio Measurements without Cluster Algorithm

It is more difficult to interpret the data correctly because of the cluster algorithm. There are particles which cross the last fibres in the edges and then fly out of the mat where the signal cannot be detected. This signal is then missing in the cluster so naturally the edges appear to have less light yield compared to the inner region.
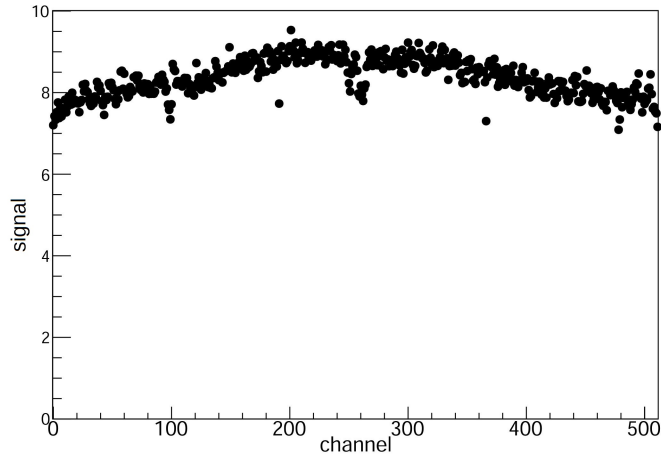

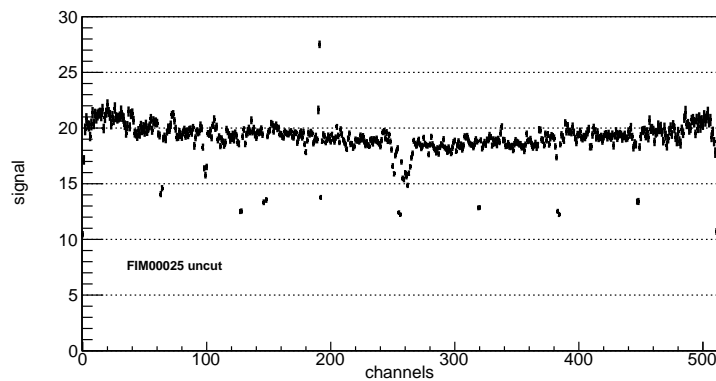Figure 5.5: Light yield of the uncut mat FIM00025 without using the cluster algorithm

Figure 5.6: Light yield of the uncut mat FIM00025 with using the cluster algorithm

Without the cluster algorithm, this is less important because we only look in the data of one channel. A threshold of three photo electrons is set for the light yield

in order to filter out the noise.

The lightyield without the cluster algorithm has a different shape. It has a slight curve what can be seen in Figure 5.5 in comparison to Figure 5.6 where the clusteralgorithm has been used.

This is because of the incident angle of the particles. Since the source is positioned at the center of the mat, the particles have a rather large angle at the edges.

In Figure 5.7 the light yield without the cluster algorithm can be seen for mat FIM00025. It is clear that compared to Figure 5.5 there are defects at the edges, so the defects must be due the process of cutting. This looked like this for all tested mats.
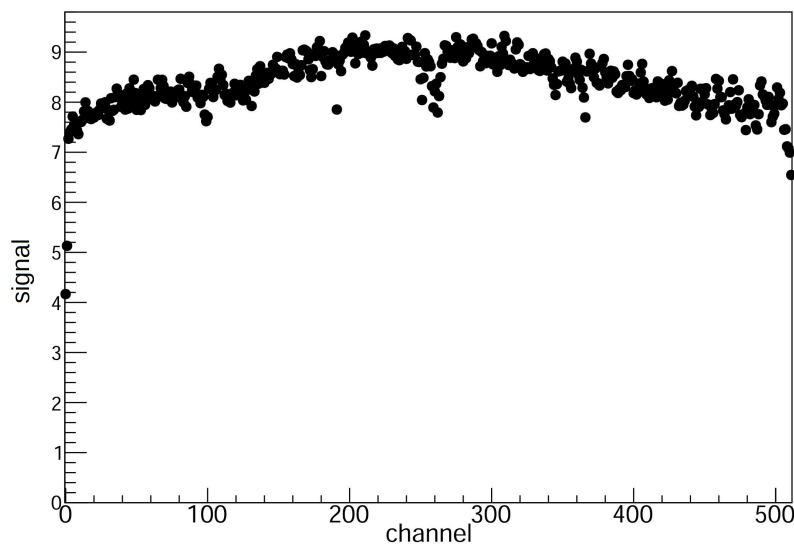

Figure 5.7: Light yield of the cut mat FIM00025 without using the cluster algorithm

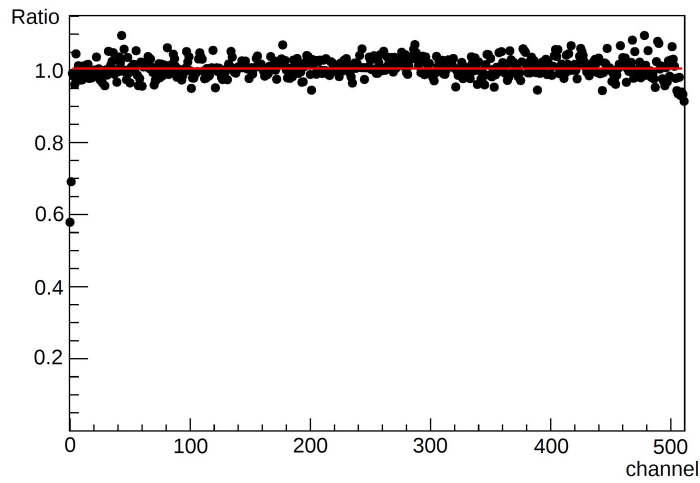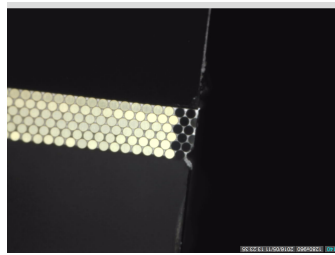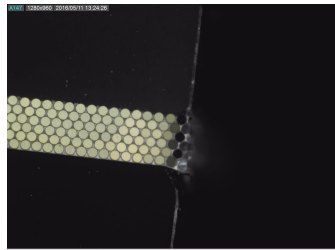In Figure 5.8 the ratio of the light yield is shown for mat FIM00025.

Figure 5.8: Ratio plot without cluster algorithm for mat FIM00025

(a) optical photo that belongs to the left edge in
the data in Figure 5.8

(b) optical photo that belongs to the right edge
in the data in Figure 5.8

Figure 5.9: Optical photo of mat FIM00025. Both pictures have the same orientaion due to camera alignments.

Looking into the optical photos in Figure 5.9, it can be seen that the data corresponds with these. As expected there are two channels affected at the left side in the data, whereas the right side looks a slightly better. But the difference between the optical photos does not seem to be as big as the difference of the light yield

data. So the optical inspection itself is not enough to give a significant evaluation of the edges of a mat.

Looking again at FIM00043, in Figure 5.10 there is the ratio displayed without the cluster algorithm. Now it is clear that the light yield for six channels at the right edge is lower but not lower than 0.6. In the measurement of the other mats it could be seen that the ratio at damaged edges got down to about 0.6. It is unrealistic that damages because of scratched fibres would always lead to the same value in the ratio. It is more likely that there is a mirror damage. So the reason why in Figure 5.3 the fibres at the edge do not reflect the light is most likely due to a mirror damage.
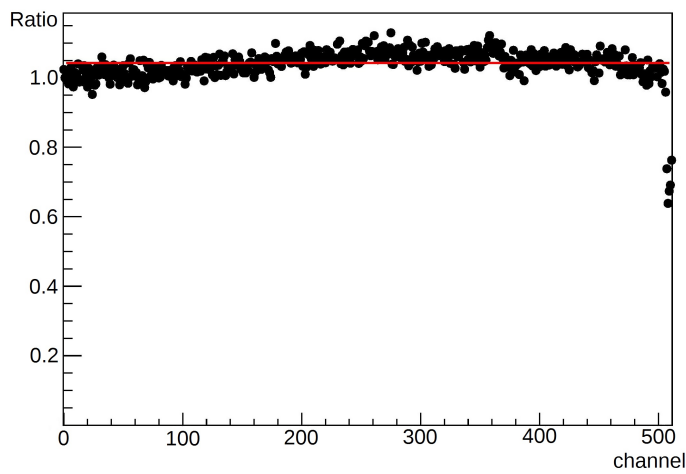

Figure 5.10: Ratio plot without cluster algorithm for mat FIM00043, the same as seen in the optical scan picture in 5.1

6 Module Measurements

6.1 Introduction

Eight of the tested fibre mats have been assembled a prototype module. Half of the module has been equipped with read-out electronics. FIM00027, FIM00028, FIM00031 and FIM00032 have been read out. These mats, especially mat FIM00028 are not

In order to detect possible defects that occurred during the process of production of the module and to improve it if necessary, measurements of the module have been made and compared to the measurements of the single fibre mats.

6.2 Experimental Setup

Figure 6.1: A photo of the setup of the prototype module

All four mats are equipped with SiPMs and front-end boards and connected to one USB Board.

In total, 16 SiPMs and four front-end boards are needed for this set-up. This leads to a read-out of 2048 channels on each side.

In this set-up a newer SiPM model, the 2015 Hamamatsu SiPMs have been used.

They provide a higher PDE of about 48%, and therefore the detected light yield will be higher.

Trigger Setup
Due to technical reasons and radiation protection, it is not so easy to have a Sr90 setup over a bigger area. Sr90 would provide particles at very high angles. This would mean that either not the full width of the module could be read-out or the source has to placed very high which lowers the rate. It is also hazardous for technicians working in the same area because they could get irradiated. Therefore, a new trigger was developed which detects cosmic rays.

A disadvantage is that triggering with cosmic rays leads to a long time for data taking. In the previous measurements it was enough to measure five minutes to already have sufficient statistics. Now, the rate only is about 8 Hz instead of over 1 kHz like in the previous set-up. This means that for reasonable data statistics, the data taking should at least take about one day. This is no problem later in serial production because it is planned to produce two to three modules in one week. That means that there is enough time for an overnight measurement for all mats with cosmic rays.
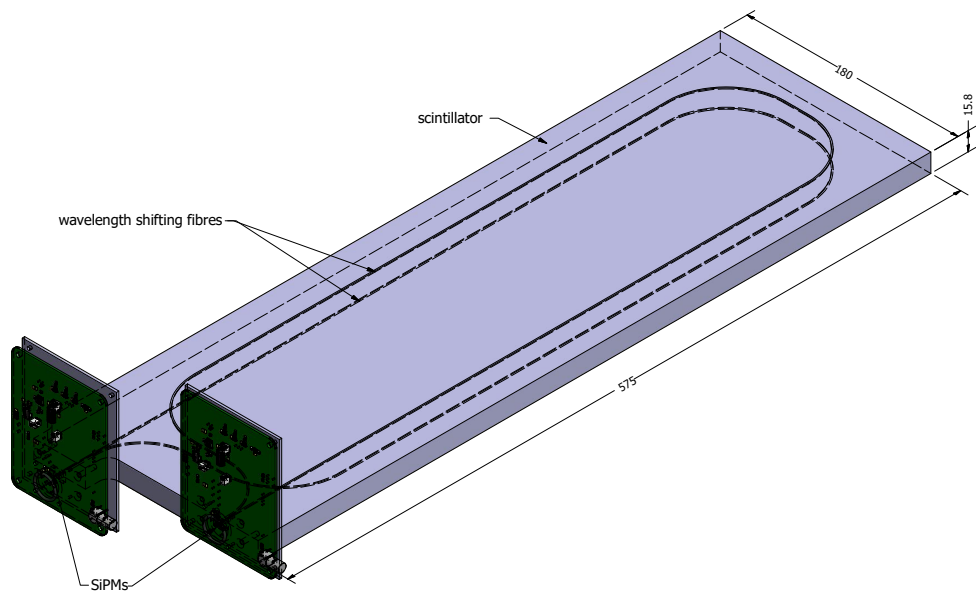

Figure 6.2: Schematic of the trigger used for the module measurements

The scintillator trigger I used in this setup is different from the one used before for the measurements in Chapter 4 and 5. It is shown in Figure 6.2.
In this new trigger, there are two wavelength-shifting fibres which are glued like an ellipsoid. Each of the fibres is connected to a single channel SiPM and read-out electronics. If a particle passes to the trigger and both fibres detect a signal, and a coincidence is formed, the USB board receives a signal that a particle was triggered.

6.3   Light Yield in Comparison

First, the light yield of one side of the module is compared with the data of the single mats in Figure 6.3 taken before with the Sr90 source (see Chapter 4) to check if any defects can be seen.
The red line is the data from one half of the module, the blue line from the single mats measurements. In Figure 6.4 also the ratio is plotted.
The structure looks similar but the light yield is about 5 photo electrons larger in the module measurements. The higher light yield of the module is due to the cosmic rays which can cross the module in much higher angles.
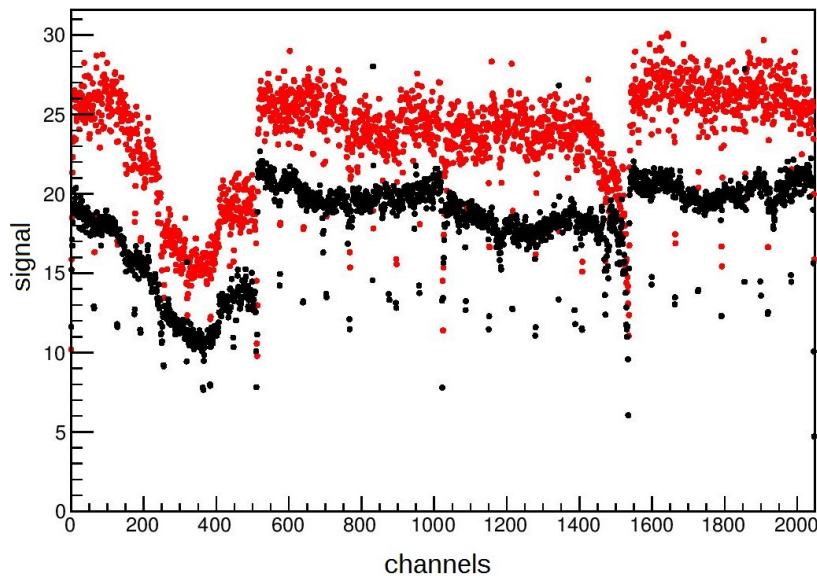

Figure 6.3: Measured light yield of the module in comparison to the light yield measured from the single mats with beta-source

Of course, the structure in Figure 6.3 does not look well and such a module could not be used later in the detector. But because with this prototype module only the procedure of the module assembling has been tested, the quality of the single

mats were not important. It is only important that the structures which could be seen with the beta-source set-up can also be seen now in the cosmic ray set-up. Therefore, also a ratio of the beta source signal and the cosmic ray signal is taken and shown in Figure 6.4.
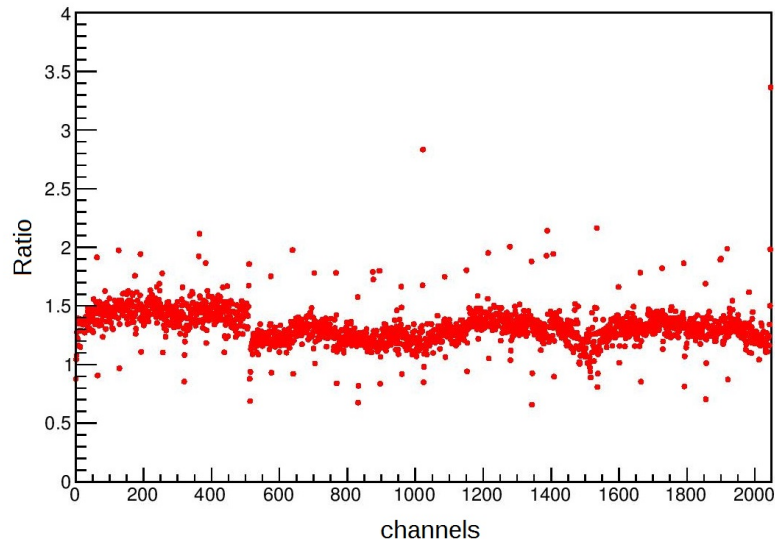

Figure 6.4: Ratio of the light yield of the module in comparison to the light yield measured from the single mats with beta-source

The ratio looks very homogeneous. This proves that the process of building the module from the mats is working good and that the read-out works fine.

6.4 Attenuation Measurement over the length

The attenuation of the light yield of the module has been measured at 10 different positions. In Figure 6.5 the measured attenuation of the light can be seen for SiPM channels 1 - 1024 (black). For these areas the light yield is homogeneous. From channel 1 to 1024 the fibre mats FIM00027 and FIM00028 are read out. For these two mats exist attenuation length measurements taken with the Sr90 set-up from Chapter 4. They are marked in blue and red in the plot. Comparing these three measurements by eye they all look similar in structure. That is a hint that the fibre mats in the module perform as good as before the assembling.
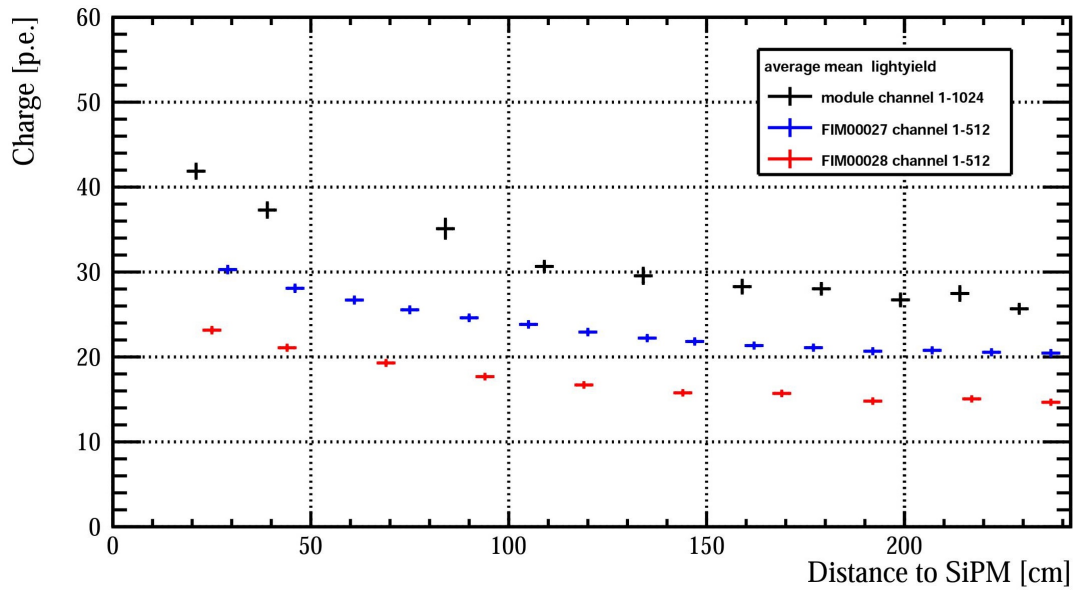
Figure 6.5: Measured attenuation over 10 different positions

The attenuation length decreases a bit and gets nearly flat from the distance of 100 cm from the SiPMs. That hints that there are no cracks or other defects during the process occurred.

7 Summary and Outlook

After the Long Shutdown of the LHC in 2019/2020, the new Scintillating Fibre Tracker (SciFi Tracker) will replace the old tracker system in the LHCb experiment. The active component of the SciFi Tracker are scintillating fibres. These fibres will be assembled into 2.5 m long and 13 cm wide fibre mats which consist of six layers of these fibres. At one end a mirror will be glued to minimize light loss, the other end is for the read-out. SiPMs (Silicon Photomultipliers) are used for the read-out. The fibre mats are produced overwidth, so the mats must be cut to the correct width by using a milling machine.

A high hit detection efficiency and a high single hit spatial tracking resolution are required for the new detector. To fulfill this, the fibre mats have to perform with a certain quality. The quality of the mats can be checked by measuring the light yield. The experience has shown that a high and homogeneous light yield is linked with a high hit detection efficiency and a high single hit spatial tracking resolution and can be measured easily under laboratory conditions.

Over 1024 fibre mats are necessary for the detector. That emphasizes how important it is to ensure good quality of the fibre mats.

It is important to test the finished fibre mats before they are built in a module because they cannot be exchanged after the mats are glued into modules. In order to guarantee that over 1024 fibre mats, which will be needed to build the SciFi detector, fulfill the requirements it is important that every mat can be checked in a short time and with adequate accurancy.

In this thesis the prototype fibre mats for the new SciFi tracker have been tested. Therefore, several things were important to check. The given light yield should be as homogeneous as possible. The edges of cut mats have to be checked because during the cutting of the fibre mats they can easily get harmed. This would lead to a sensitive loss of signal. Also, the mirror can get damaged during the process of production. This can be also seen in the light yield. To verify the quality of the mats there is a set of tests that can be carried out. In this thesis the light yield measurements before and after the mat is cut and the optical inspection after the cut and the attenuation measurements over the length of the mat/module are described.

With these tests some difficulties in production could be discovered and corrected. For example, the glue-type for the alignment pins of the fibre mats has been changed after seeing in the data that fibres have been damage due to it. An important consequence of these measurements is, that the technique for the longitudinal cuts has to be refined to avoid damages of the mirror or fibres. That this damages have been found by analyzing the measured data is a good sign, that the measurements provide enough sensibility.

A comparison of the prototype module with the single fibre mat measurements

showed no significant deterioration of their performance, indicating that the assembling of modules works well.

In the future, serial production will start and these measurements will be taken for every produced fibre mat to rank them in quality to decide if they will be build in a beam-near module or not, to sort them out if necessary.

8   References

References

[1] The LHCb Collaboration, *LHCb Tracker Upgrade Technical Design Report*, CERN/LHCC 2014/001, LHCb TDR 15, Feb 2014.

[2] The LHCb Scintillating Fibre Tracker Collaboration, *LHCb Scintillating Fibre Tracker Test Beam Report 2015*, LHCb-PUB-2015-025, Jun 2016.

[3] The LHCb Collaboration, *The LHCb Detector at the LHC*, 2008.

[4] H. Satz, *Großforschung in neuen Dimensionen*, Springer Spektrum, 1st edition, 2016.

[5] B. Saleh, M. Teich, *Fundamentals of photonics*, Wiley, 2007.

[6] M. Grundmann, *The physics of semiconductors*, Springer, 2nd ed., 2010.

[7] W. Demtröder, *Experimentalphysik 4 Kern-, Teilchen-, Astrophysik*, Springer Sprektrum, 4th ed., 2014.

[8] The LHCb Scintillating Fibre Collaboration, *LHCb Scintillating Fibre Tracker Engineering Design Review Report: Fibres, Mats and Modules*, LHCb-PUB-2015-008, Jul 2015.

[9] `http://phys.org/news/2015-05-particle-physics-discovery-theory.html`, 01.09.2016, 13.00 pm.

[10] The LHCb collaboration, *Framework TDR for the LHCb Upgrade*, CERN/LHCC 2012-007, LHCb TDR 12, May 2012.

[11] H. Chanal, A. Comerma, M. Deckenhoff, D. Gascón, S. Gómez, C. Joram, G. Haefeli, X. Han, J. Mazorra de Cos, P. Perret, N. Pillet, R. Vandaële, U. Uwer, *LHCb Scintillating Fibre Tracker Engineering Design Review: PACIFIC Readout ASIC*, Apr 2016.

[12] H. Kolanoski, *Teilchendetektoren*, Springer Spektrum, 1st ed., 2016.

[13] P. Mouche, Overall view of the LHC, OPEN-PHO-ACCEL-2014-001, `https://cds.cern.ch/record/1708847/?ln=de`, 18.09.2016, 18.00 pm.

[14] `http://multimedia.3m.com/mws/media/12450890/3m-enhanced-specular-reflector-films-3m-esr-tech-data-sheet.pdf`, 19.09.2016, 9.00am.

Erklärung

Ich versichere, dass ich diese Arbeit selbstständig verfasst und keine anderen als die angegebenen Quellen und Hilfsmittel benutzt habe.

Heidelberg, den 19.09.2016,

....